Epitaxy-Driven Synthesis of Elemental Ge/Si Strain-Engineered Materials and Device Structures via Designer Molecular Chemistry

ARTICLE *in* CHEMISTRY OF MATERIALS · NOVEMBER 2007

Impact Factor: 8.35 · DOI: 10.1021/cm071581v

7 AUTHORS, INCLUDING:

Yina Fang
Huazhong University of Science and Techn…
54 PUBLICATIONS **763** CITATIONS
SEE PROFILE

John Tolle
ASM International N.V.
126 PUBLICATIONS **1,681** CITATIONS
SEE PROFILE

Jesse B Tice
Arizona State University
11 PUBLICATIONS **93** CITATIONS
SEE PROFILE

Vijay Richard D'Costa
National University of Singapore
60 PUBLICATIONS **812** CITATIONS
SEE PROFILE

CHEMISTRY OF MATERIALS

Article

Epitaxy-Driven Synthesis of Elemental Ge/Si Strain-Engineered Materials and Device Structures via Designer Molecular Chemistry

Y.-Y. Fang, J. Tolle, Jesse Tice, A. V. G. Chizmeshya, J. Kouvetakis, V. R. D'Costa, and José Menéndez

Chem. Mater., **2007**, 19 (24), 5910-5925• DOI: 10.1021/cm071581v • Publication Date (Web): 24 October 2007

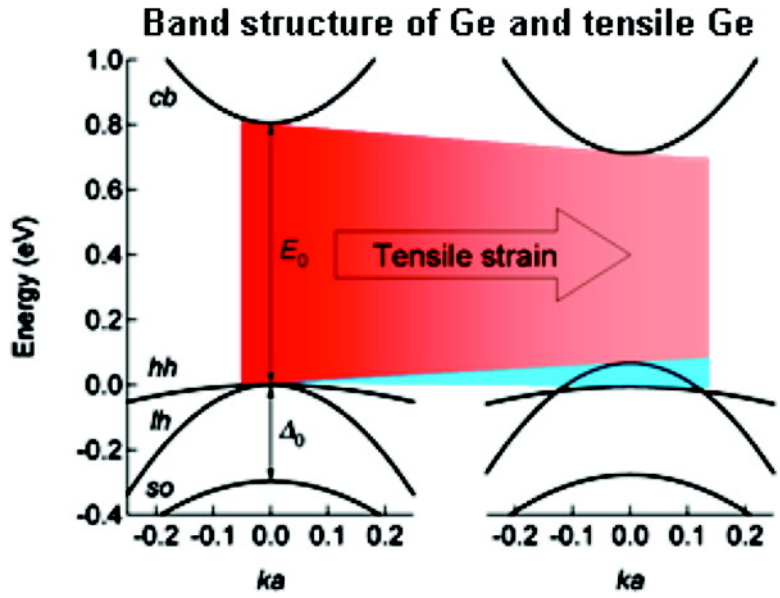

More About This Article

Additional resources and features associated with this article are available within the HTML version:

- Supporting Information
- Links to the 2 articles that cite this article, as of the time of this article download
- Access to high resolution figures
- Links to articles and content related to this article
- Copyright permission to reproduce figures and/or text from this article

View the Full Text HTML

Chemistry of Materials is published by the American Chemical Society. 1155 Sixteenth Street N.W., Washington, DC 20036

Epitaxy-Driven Synthesis of Elemental Ge/Si Strain-Engineered Materials and Device Structures via Designer Molecular Chemistry

Y.-Y. Fang,[†] J. Tolle,[†] Jesse Tice,[†] A. V. G. Chizmeshya,[†] J. Kouvetakis,*[,†] V. R. D'Costa,[‡] and José Menéndez*[,‡]

Department of Chemistry and Biochemistry and Department of Physics and Astronomy, Arizona State University, Tempe, Arizona 85287

Received June 13, 2007. Revised Manuscript Received August 15, 2007

We describe the systematic epitaxial engineering of device-quality elemental structures in the Ge/Si system. By introducing small concentrations of $(GeH_3)_2CH_2$ or GeH_3CH_3 organometallic additives into conventional Ge_2H_6, we have developed several new low-temperature CVD growth strategies that permit heteroepitaxy of highly dissimilar materials and provide unprecedented control of film microstructure, morphology, composition, and tuning of optical properties. Optimized molecular mixtures of these compounds have enabled layer-by-layer growth via facile elimination of extremely stable CH_4 and H_2 byproducts, consistent with calculated chemisorption energies and surface reactivities. Collectively, our experiments indicate that the additives confer unique pseudosurfactant behavior that profoundly alters the classic Stranski–Krastanov growth mechanism of epitaxial Ge on Si surfaces. Using this approach, we have produced atomically smooth, carbon-free Ge layers directly on Si with dislocations densities less than 1×10^5 cm^{-2} (significantly less than those attainable from the best competing processes) at unprecedented low temperatures (350–420 °C) compatible with selective area growth applications. Full relaxation of the film is readily achieved via formation of Lomer dislocations confined to the Ge/Si interface, which should, in principle, allow film dimensions approaching bulk values to be achieved on a Si substrate. Here, films with thicknesses up to several micrometers have been grown for use as passive/active heterostructure components. The practical utility of the approach is demonstrated for the first time by growing pure Ge seamlessly, conformally, and selectively in the "source/drain" regions of prototypical device structures. This innovation represents an ultimate extension of uniaxial strain techniques using group IV materials and is likely to have applications in the integration of microelectronics with optical components (photodiodes) into a single chip. As an additional example for high-mobility device template application, we have grown tensile Si films on the Ge buffers via decomposition of $SiH_3SiH_2SiH_3$. The new Ge growth processes also provide a unique route to extend the utility of elemental Ge into the wider IR optoelectronic domain by tuning its fundamental optical properties using tensile strain as a main parameter. In this study, we use the metal–organic additives to circumvent traditional surface-energy limitations and produce for the first time high-quality, thermally stable, tensile strained Ge layers at low temperature (350–380 °C) on $Ge_{1-y}Sn_y$-buffered Si(100). The precise strain state of the epilayers is controlled by varying the Sn content of the buffer, yielding tunable record-high tensile strains as high as 0.43%. This strain-tuning strategy may offer the prospect of producing direct optical gaps in elemental Ge.

Introduction

Innovations in epitaxy over the past three decades have made it possible to increase the versatility of semiconductor materials by inducing quantum confinement, applying strain, and creating device designs based on mismatched materials with engineered defect structures grown under metastable conditions. The next generation of high-performance silicon technologies will undoubtedly require extensive integrations of dissimilar materials in device-quality architectures, as well as precise tuning of the associated structural strains. In the topical Si–Ge arena, new materials and creative strained-layered designs have already led to higher speeds in microprocessors,[1] lower power consumption in cell phones,[2] advances in silicon-based photonics,[3] and more efficient solar cells.[4] Our recent work in this area focuses on the use of CVD to enable fabrication of unique epitaxial structures using designer molecular hydrides.

One recent example of our precursor-driven synthesis is the demonstration of a generalized low-temperature deposition of atomically smooth and stress-free Ge films directly on Si at the unprecedented range of 350–420 °C.[5] Using the same approach we have been able to reproduce the highest

* Corresponding author. E-mail: jkouvetakis@asu.edu.
[†] Department of Chemistry and Biochemistry, Arizona State University.
[‡] Department of Physics and Astronomy, Arizona State University.

(1) Luryi, S.; Xu, J.; Zaslavsky, A. *Future Trends in Microelectronics: Up the Nanocreek*; Wiley: New York, 2007.
(2) Heftman, G.; Grossman, S.; Day, J. *Power Electron. Technol.* **2005**, 44.
(3) Jalali, B.; Paniccia, M.; Reed, G. *IEEE Microwave Mag.* **2006**, *7*, 1440.
(4) Green, M. A. *Progr. Photovoltaics* 20019, 123.
(5) Wistey, M. A.; Fang, Y.-Y.; Tolle, J.; Chizmeshya, A.V.G.; Kouvetakis, J. *Appl. Phys. Lett.* **2007**, *90* (8), 082108.

10.1021/cm071581v CCC: $37.00
Published on Web 10/24/2007

reported Ge tensile strains by growing the material on our hybrid $Ge_{1-y}Sn_y$/Si(100) substrates, which provide a growth platform that possesses the required larger lattice dimension than that of Ge.[6] In both cases, we routinely obtain layers with atomically flat surfaces and extremely low threading dislocation densities below 1×10^5 cm^{-2}, orders of magnitude less than those attainable from the best competing process available for Ge on Si structures. The desirable growth conditions and superior morphology and microstructure (low threading dislocation densities) make these materials suitable for applications in selective growth, MOSFETs, HBTs, optoelectronic devices, and III/V integration on Si.

Stress-Free Ge on Si Structures. Elemental Ge with a stress-free microstructure has a small (0.7 eV) indirect gap and a slightly larger (0.8 eV) direct gap (E_0). The resulting small effective masses find applications in high-mobility transistors.[7,8] The optical absorption features a sharp rise at the direct gap, covering a spectral range of interest for optical communications. This overlap has generated strong interest in Ge-based infrared photodetectors[9,10] and optical modulators.[11] For these high-speed applications, the Ge epilayer must be flat—to enable submicron lithography—and possess device-quality defect concentrations. These properties can be achieved to some extent in recently developed processes conducted via a modified ultrahigh vacuum chemical vapor deposition (UHV-CVD) technique and via molecular beam epitaxy (MBE). In either case, however, it is necessary to introduce an intermediate buffer layer to accommodate the inherent 4% strain differential between the Si substrate and the Ge epilayer. Alternatively, one must develop conditions that reduce the surface energies, ultimately leading to desirable growth morphologies.

Growth of Ge on Si typically proceeds via the Stranski–Krastanov mechanism, yielding islands (after deposition of 3–4 monolayers) rather than relaxed, continuous layers. For thick films, a high roughness is obtained and threading dislocation densities of $\sim 1 \times 10^8$ cm^{-2} are commonly observed, eventually producing the classic cross-hatched surface morphologies.[12] Scattering and traps at defect sites reduce carrier mobility in electronic devices and increase dark current in photodetectors. A variety of growth schemes have been developed in an attempt to circumvent some of these problems, including (i) the use of a graded Si–Ge buffer layer,[12] (ii) a two-step growth in which an initial thin buffer layer is deposited at low temperature, followed by the high-temperature growth of the bulk material,[13] and (iii) surfactant-mediated epitaxy using As and Sb atomic beams.[14] The compositionally graded $Si_{1-x}Ge_x$ buffer layer approach has been demonstrated via UHV-CVD. The Ge concentration is gradually increased as a function of layer thickness, and the terminal Ge portion of the stack exhibits a defect density of 1×10^7 cm^{-2} and a high AFM rms roughness of 50 nm. A post-growth-chemical mechanical polishing step is then conducted to reduce the surface roughness to a level that allows subsequent growth of lower defect density overlayers of the Ge material. The drawbacks of this method include excessive final film thicknesses (~ 11 μm) and a relatively large residual surface roughness, both of which are problematic for device fabrication. An alternative two-step UHV-CVD process has also been developed (current state-of-the-art) to produce relaxed Ge on Si films with relatively flat surfaces. Here, an initiation layer of $\sim$ 50 nm in thickness is first grown at low temperatures of $\sim$350 °C. This layer is intended to facilitate subsequent bulk growth at higher temperatures of $\sim$800–900 °C and significantly enhanced rates. In this process, the excess hydrogen on the growth surface is believed to act as a surfactant, thereby promoting the formation of misfit dislocations parallel to the Ge–Si interface, which relieves the misfit strain. The surface morphology of the resultant films reveals an AFM rms roughness value of 0.5 nm with no sign of the cross-hatch pattern attributed to strain relaxations. However, defect densities of 2.3×10^7 cm^{-2} are purportedly present even after thermal cycling of the samples between 780 and 900 °C. Further reductions in defect densities to levels as low as $\sim 2 \times 10^6$ cm^{-2} can be obtained using this method via selective growth on oxide patterned Si wafers.[13] In recent years, more conventional surfactant-based approaches have been implemented via MBE to grow Ge layers with suitable morphologies using solid sources of As or Sb. This is typically achieved by first depositing a completed surfactant monolayer on clean Si prior to growth of pure Ge. Using this method, researchers have demonstrated ~ 1 μm Ge thick films with defect densities of $\sim 2 \times 10^7$ at 700 °C (the surface roughness was not reported in this case).[14] The resultant films have been found to exhibit tensile strains as high as 0.2% because of the thermal mismatch with the Si substrate. They are also unintentionally doped by the As/Sb surfactant.

The above issues have prompted us to consider an alternative, more straightforward approach that circumvents the complexity of the two-step high-temperature processing, obviates the need for thick Si–Ge buffers, and is not affected by the unintentional incorporation of residual impurities. Our approach is based on the design and application of purpose-built molecular precursors targeted to tailor the surface reactions at the growth front. This is achieved by the deposition of highly reactive compounds such as $(GeH_3)_2CH_2$ digermylmethane (Figure 1) with built-in "pseudosurfactant" capabilities intended to promote layer-by-layer growth of smooth, continuous and relaxed Ge films devoid of deleteri-

(6) Fang, Y.-Y.; Tolle, J.; Roucka, R.; Chizmeshya, A. V. G.; Kouvetakis, J.; D'Costa, V. R.; Menendez, J. *Appl. Phys. Lett.* **2007**, *90* (6), 061915.
(7) Oh, J.; Campbell, J. C.; Thomas, S. G.; Bharatan, S.; Thoma, R.; Jasper, C.; Jones, R. E.; Zirkle, T. E. *IEEE J. Quantum Electron.* **2002**, *38*, 1238.
(8) Lee, M. L.; Fitzgerald, E. A.; Bulsara, M. T.; Currie, M. T.; Lochtefeld, A. *J. Appl. Phys.* **2005**, *97*, 11101.
(9) Jutzi, M.; Berroth, M.; Wohl, G.; Oehme, M.; Kasper, E. *IEEE Photonics Technol. Lett.* **2005**, *17*, 1510.
(10) Liu, J. F.; Michel, J.; Giziewicz, W.; Pan, D.; Wada, K.; Cannon, D. D.; Jongthammanurak, S.; Danielson, D. T.; Kimerling, L. C.; Chen, J.; Ilday, F. O.; Kartner, F. X.; Yasaitis, J. *Appl. Phys. Lett.* **2005**, *87*, 103501.
(11) Kuo, Y. H.; Lee, Y. K.; Ge, Y. S.; Ren, S.; Roth, J. E.; Kamins, T. I.; Miller, D. A. B.; Harris, J. S. *Nature* **2005**, *437*, 1334.
(12) Fitzgerald, E. A.; Samavedam, S. B. *Thin Solid Films* **1997**, *294*, 3.
(13) Luan, H.-C.; Lim, D. R.; Lee, K. K.; Chen, K. M.; Sandland, J. G.; Wada, K.; Kimerling, L. C. *Appl. Phys. Lett.* **1999**, *75*, 2909.
(14) Wietler, T. F.; Bugiel, E.; Hofmann, K. R. *Appl. Phys. Lett.* **2005**, *87*, 182102.

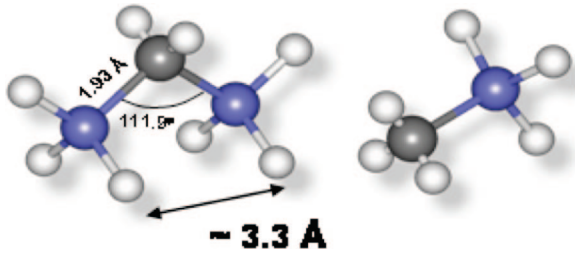

Figure 1. Structures of $(GeH_3)_2CH_2$ and GeH_3CH_3. Note that the Ge–Ge dimension in the former is close to the distance of Ge sites on cubic a Ge (100) orientation, enabling facile adsorption of the compound on the growing Ge surface. The Ge, C, and H atoms are represented by blue, grey, and white spheres, respectively.

ous threading dislocations. The driving force for the deposition reactions of this compound is the facile desorption of extremely robust CH_4 byproducts, leading to the complete elimination of carbon from the precursor. In a brief Communication, [5] we recently reported proof-of-concept studies that produced Ge layers with record-low threading dislocation densities $<1 \times 10^5/cm^2$. These films are obtained by reacting suitable molar concentrations of $(GeH_3)_2CH_2$ in Ge_2H_6. A key observation is that the films produced with thickness up to 0.8 μm are fully relaxed. Accordingly, there is in principle no upper bound on the thickness achievable by this low-temperature process.

In this paper, we describe in detail the growth procedure and the surface reaction thermodynamics leading to the growth of thick Ge films on Si. The pseudo surfactant action of the $(GeH_3)_2CH_2$ compound is addressed using quantum chemical simulations. The main objective of this ongoing work is to produce the lowest possible concentration of penetrating defects in atomically flat, 1–10 μm thick films with chemically abrupt heterointerfaces and demonstrate selective growth of the material in complex device architectures for high mobility applications. The ultimate goal is to produce advanced templates for integration of a variety of thermally and structurally mismatched semiconductors such as III–Vs with Si. As an example of an advanced application of this process, we demonstrate the growth of metastable tensile-strained and fully pseudomorphic Si films on Ge buffers using trisilane as the source of silicon.

The success of the $(GeH_3)_2CH_2/Ge_2H_6$ approach prompted us to explore deposition reactions using the simpler, inexpensive, and more readily available analog GeH_3CH_3 (Figure 1), which is likely to follow a similar decomposition mechanism driven by the release of CH_4, ultimately leading to pure Ge films at even lower temperatures. Depositions based on appropriate, minor concentrations of GeH_3CH_3 in a Ge_2H_6 mixture were conducted on a single-stage wafer configuration at very low temperatures (360 °C), which precluded any side reactions that might lead to carbon contamination. This method consistently yielded perfectly epitaxial films with atomically flat surfaces and fully relaxed microstructures devoid of penetrating, threading dislocations. The films were totally free of carbon impurities, indicating stoichiometric dissociation of the compound according to the equation: $GeH_3CH_3 \rightarrow Ge + H_2 + CH_4$.

In general, we find that mixtures comprising either GeH_3CH_3 or $(GeH_3)_2CH_2$ gaseous samples combined with a large excess of commercially available Ge_2H_6 provide a novel and practical route to low-temperature depositions of Ge-based structures with microstructural and morphological quality that cannot be obtained by conventional routes. In this study, we compare and contrast our Ge deposition products obtained using both of these closely related compounds, on the basis of growth characteristics, reaction kinetics, strain, microstructure, and bonding properties. The material quality is corroborated with well-established optical methodologies including Raman, photoluminescence, and photoreflectance. Collectively, our experiments demonstrate that small concentrations of the $(GeH_3)_2CH_2$ and GeH_3CH_3 organometallic additives can profoundly alter the classic Stranski–Krastanov growth mechanism of epitaxial Ge films on mismatched Si surfaces.

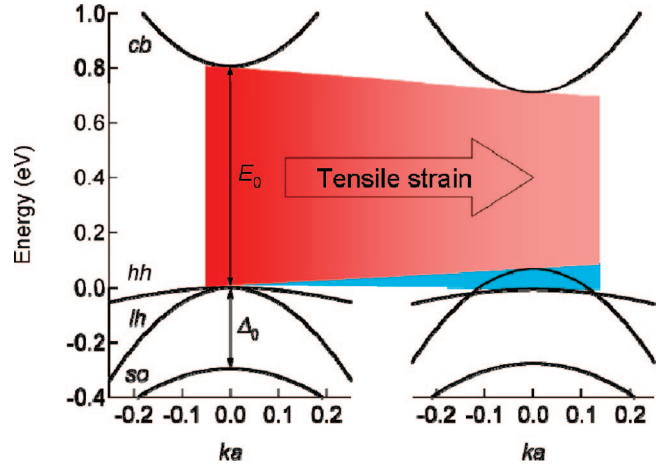

Figure 2. Electronic band structure of Ge near the lowest direct band gap E_0. Here, k is the wave vector along the <100> direction, and a the cubic lattice constant. The bands are indicated as *cb* (conduction band), *hh* (heavy hole band), *lh* (light hole), and *so* (split off band). The valence band spin–orbit splitting at $k = 0$ is Δ_0. The right panel shows the bands calculated for a tensile strain of 1% using absolute deformation potentials. The strain dependence of the effective masses was ignored. The zero energy is chosen at the top of the valence band in the unstrained case (left panel).

Tensile-Strained Ge Structures. In addition to stress-free films, this study describes the growth and properties of tensile-strained analogs. These materials represent a new semiconductor system that is distinct from those in which the strain is a byproduct of uncontrolled growth or thermal processing. Here, we synthesize tetragonal Ge polymorphs via large, epitaxially induced strains on the parent diamond structure. One immediate goal is to further extend the utility of Ge into the wider infrared optoelectronic domain by tuning its fundamental optical properties using strain as a main parameter. The degree of tensile strain alters the Ge band structure and induces a tunable redshift of the direct gap E_0 absorption edge. Figure 2 shows the quantitative changes in the band structure for 1% tensile strain in Ge. Small reductions in E_0 can dramatically improve the detection performance of this material at 1.55 μm and beyond to cover the technologically important near-IR telecom bands for use in optical fiber communications. For sufficiently large tensile strain, it has been predicted that Ge will become a direct gap

system,[15] with potential applications as an active lasing material. This was recognized almost 10 years ago by Soref and Friedman,[16] who proposed that hypothetical $Ge_{1-y}Sn_y$ alloys containing up to 11% Sn could serve as buffer layers to produce these strain states and lead to the realization of novel devices such as Si-based *p–i–n* injection lasers based on Ge(tensile)/$Ge_{1-x}Sn_x$/Si(100) stacks.

The challenge with respect to materials synthesis in this area is the development of methodologies that would enable precise control of tunable strains for device design purposes. On fundamental grounds, pseudomorphic epitaxy via templates based on the C–Si–Ge compositional sequence cannot be used to induce a tensile strain state in Ge, because the latter already possesses the largest lattice constant. However, by growing Ge directly on Si at 800 °C and taking advantage of the smaller thermal expansion coefficient of the substrate, researchers have induced tensile strain in the Ge epilayer upon cooling the heterostructure to room temperature.[17,18] This has produced a maximum reported strain value on the order of 0.25% in films as thick as 1μm, which is sufficient for some photodetector designs but not suitable for most optoelectronic applications that require tunable direct gaps.[19] In the context of laser applications, spatial confinement requires abrupt interfaces, which are precluded using this high-temperature process because of the inherent elemental intermixing at the interface. In addition, precise and systematic control of the final strain state has not been demonstrated using this method, which hampers the design of devices.

To address these issues, we have developed a rational approach based on the creation of $Ge_{1-y}Sn_y$ alloys with tunable lattice dimensions above that of Ge, which serve as the critical facilitating platforms for the subsequent tensile Ge growth. In addition, this approach subsumes the following distinctive features: (i) low growth temperature that promotes the assembly of highly strained tetragonally distorted Ge structures that remain robust despite the inherent metastability; (ii) layer-by-layer growth mechanisms leading to flat surfaces, chemically abrupt interfaces devoid of chemical intermixing, and relatively defect free layer microstructures. Both features are enabled by exploiting the high reactivity and the peudosurfactant behavior of the $(GeH_3)_2CH_2$ or GeH_3CH_3 species. Collectively, this methodology has allowed us to systematically produce Ge layers with very high tensile strains and all of the desired morphological and structural properties as discussed below.

Experimental Section

General Deposition Procedures. The Ge films were grown directly on Si by gas source molecular beam epitaxy (GS-MBE) at 350–420 °C and 5×10^{-5} Torr using admixtures of either $(GeH_3)_2CH_2$ or GeH_3CH_3 and Ge_2H_6 at optimized molar ratios. The reaction mixture was prepared prior to each deposition by combining the pure compounds in a 100 mL vacuum flask. The total pressure was 115 Torr, which is well below the vapor pressure of $(GeH_3)_2CH_2$ (248 Torr at 25 °C) or GeH_3CH_3,which is a gas at room temperature. The flask was connected to a gas injection manifold that was pumped to $\sim 1 \times 10^{-8}$ Torr on the gas source MBE chamber. A boron-doped (1–10 Ω cm) Si (100) wafer was RCA cleaned and then cleaved to a 1 cm^2 size that fits the dimensions of the sample stage. Each substrate was sonicated in methanol for 5 min, dried under a stream of purified N_2, and inserted through a load lock into the MBE chamber at a base pressure of 8×10^{-10} Torr. The sample was then heated at 600 °C under UHV to remove surface contaminants until the pressure of the chamber was restored to background levels. The sample was subsequently flashed 10 times to 1000 °C for 1 s to remove any remaining contaminants, and then flashed again at 1150 °C for 5 times to remove the native oxide from the silicon. To commence growth, we heated the wafer to 350–420 °C as measured by single-color pyrometer and the temperature was then allowed to stabilize for 5 min. The heating was performed by passing direct current though the samples. The precursor mixture was introduced into the chamber at a flow rate of approximately 0.08 sccm through a manual leak valve. The pressure was maintained at a constant rate (5×10^{-5} Torr) during growth via dynamic pumping using a corrosion-resistant turbomolecular pump. The typical deposition times were 0.5–5 h depending on the desired film thickness. Under these conditions, Ge on Si films were produce with thicknesses in the range of 0.30–3 μm at rates approaching 10 nm/min.

Structural and Optical Characterization. The samples were extensively characterized for morphology, microstructure, purity, and crystallographic properties by atomic force microscopy (AFM), Rutherford backscattering (RBS), secondary ion mass spectrometry (SIMS), cross-sectional transmission electron microscopy (XTEM), and high-resolution X-ray diffraction (XRD). The threading defects densities were estimated using an etch pit technique (EPD).

Raman studies were carried out at room temperature using several laser lines. The laser beam was focused on the sample using a 100× objective. Typical incident powers were in the 1–2 mW range. The scattered light was dispersed with either an Acton 27.5 cm or an Acton 50.0 cm spectrometer equipped with 1800 and 2400 grooves/mm gratings and charge-coupled device detectors. Photoreflectance experiments were performed at room and cryogenic temperatures using a laser wavelength of 514.5 nm. The modulating laser beam was chopped at 1 kHz. Light from a quartz tungsten halogen source was reflected off the sample, dispersed through the Acton spectrometer, and focused on an InGaAs detector. The AC component of the signal was extracted using standard lock-in techniques. The same setup minus the halogen lamp was used for photoluminescence experiments.

State-of-the-art Raman instruments are capable of detecting atomically thin semiconductor films. This, combined with the well-known chemical and strain sensitivity of Raman spectroscopy, makes Raman scattering an ideal technique to complement X-ray strain studies, particularly in those cases in which minute amounts of material are present or the superposition of different layers with similar lattice constants makes it difficult to extract quantitative information from XRD. The first-order Raman spectrum of diamond semiconductors consists of a single peak corresponding to the triply degenerate optical phonons at the center of the Brillouin zone, which in all these materials (except diamond itself) represents the highest frequency vibrations in the lattice. The application of strain removes the degeneracy of the three optical modes. The new frequencies

(15) Menendez, J.; Kouvetakis, J. *Appl. Phys. Lett.* **2004**, *85*, 1175.
(16) Soref, R. A.; Friedman; L., *Superlattices Microstruct.* **1993**, *14* (213), 189.
(17) Ishikawa, Y.; Wada, K.; Cannon, D. D.; Liu, J.; Luan, H.-C.; Kimerling, L. C. *Appl. Phys. Lett.* **2003**, *82*, 2044.
(18) Cannon, D. D.; Liu, J.; Ishikawa, Y.; Wada, K.; Danielson, D. T.; Jongthammanurak, S.; Michel, J.; Kimerling, L. C. *Appl. Phys. Lett.* **2004**, *84*, 906.
(19) Liu, J.; Cannon, D. D.; Wada, K.; Ishikawa, Y.; Danielson, D. T.; Jongthammanurak, S.; Michel, J.; Kimerling, L. C *Phys. Rev. B* **2004**, *70*, 155309.

and eigenvectors can be calculated as an exercise in degenerate perturbation theory.[20] For diamond-structure films that grow on lattice mismatched substrates or buffer layers along the <001> crystal direction, there is a mismatch strain ($\epsilon_{||}$) in the plane of the growing surface, and from elasticity theory the strain in the vertical growth direction is $\epsilon_{\perp} = (-2C_{12}/C_{11})\epsilon_{||}$, where C_{11} and C_{12} are the elastic constants. This strain splits the zone-center modes into a doublet with in-plane atomic displacements and a singlet with atomic displacements along the growth direction. For the typical backscattering configuration used in Raman scattering from opaque materials, only the singlet is observed. Thus the Raman spectrum displays a single, strain-shifted peak instead of a double-peak structure. The strain shift of the singlet mode can be written as[20]

$$\Delta\omega = b\epsilon_{||} \quad (1)$$

where b is the so-called strain-shift coefficient. For Si and Ge, the strain shift coefficients were determined in the early 70s from Raman measurements of bulk samples under uniaxial stress.[21,22] These experiments were performed with visible laser lines and yielded $b_{Si} = -720 \pm 140$ cm^{-1} and $b_{Ge} = -415 \pm 40$ cm^{-1}. The negative sign indicates that the Raman frequencies decrease for tensile strain. A laser wavelength dependence of phonon strain coefficients is not expected, but it has been found experimentally for a number of materials, as summarized in ref 23. The standard explanation is based on the fact that the volume probed by Raman experiments moves closer to the sample surface as the optical absorption increases. Thus for any strain relaxation near the surface, measurements with short laser wavelengths might yield artificially small phonon deformation potentials. More recent experiments using longer wavelengths appear to confirm this scenario. In the case of Si, for example, measurements with a 1064 nm laser line[23] yield $b_{Si} = -830 \pm 40$ cm^{-1}. No such measurements have been performed for Ge, because Raman instruments operating at photon energies below the absorption edge of Ge are not standard.

The development of strained-layer epitaxy provided a new tool to determine phonon strain coefficients using well-characterized samples. The amount of strain is typically much larger than in bulk samples under macroscopic stresses. For sufficiently thin layers, the near-surface strain is not relaxed and, in addition, the Raman signal originates from the entire film. Therefore, one does not expect to observe the laser wavelength dependencies found in stress experiments. For Si, Nakashima and co-workers[24] find $b_{Si} = -723 \pm 15$ cm^{-1} at 244 nm and $b_{Si} = -733 \pm 10$ cm^{-1} at 488 nm, in agreement with these expectations.

It is interesting to note that the strain-shift coefficient for Si determined from thin film measurements is in agreement with the earlier stress measurements with visible wavelengths but about 10% smaller than the presumably more accurate value obtained with infrared excitation. The reason for this discrepancy is not known, but the results suggest that a thin film determination of the strain shift coefficient in Ge would be highly desirable. To the best of our knowledge, such measurements have not been reported, perhaps because of the scarcity of experiments using layers of pure Ge under epitaxial strain. Our fabrication of well characterized tensile-strained Ge films as described below make it possible to carry out these measurements. In this paper, we confirm that the strain shift coefficient of Ge measured by Cerdeira et al.[21] for bulk samples is adequate for epitaxially strained films.

Results and Discussion

Strain-Free Ge Growth via $(GeH_3)_2CH_2$. At the onset of the deposition experiments, we systematically varied the substrate temperature and the reactant concentration in the gaseous mixture to determine the optimum growth parameters and the most favorable surface reaction conditions that would yield the best possible film quality in terms of purity, morphology, and microstructure. We found that the ratio of the $(GeH_3)_2CH_2/Ge_2H_6$ precursor flux had a profound effect on all of these material properties. For example, growth using molar ratios in the range form 1:2 to 1:5 produced discontinuous layers with rough surfaces dominated by islands of variable size and shape. These samples were analyzed by RBS carbon resonance profiles, which revealed a significant carbon contamination throughout the layers, primarily in samples grown using molecular ratio of 1:2 and 1:5. This indicates that in such highly concentrated mixtures, the pseudosurfactant reaction mechanism of the $(GeH_3)_2CH_2$ compound, which is designed to proceed with complete elimination of the CH_2 fragment as CH_4, is compromised, resulting in the incorporation of residual C–H impurities. Further reduction of the compound molar ratio in the range of 1:10 to 1:15 yielded higher-purity, carbon-free films with atomically smooth surfaces (AFM rms values of 0.3 nm) and thickness up to $\sim$3 μm. Under these conditions, the growth rate and film thickness were found to depend sensitively on the growth temperature. More specifically, between 430 and 350 °C, the nominal rates and corresponding thicknesses were 10–5 nm/min and 3–0.8 μm, respectively, and no discernible growth was observed below 350 °C. It is interesting to note that deposition reactions in the range of 450–470 °C produced films that were contaminated with carbon at levels as high as several atomic percent and exhibited relatively rough surfaces with rms values or 3–5 nm. This is consistent with previous UHV-CVD experiments of the related GeH_3CH_3 compound, which yielded similar carbon incorporations.

Finally, we also conducted control experiments using pure Ge_2H_6 (in the complete absence of $(GeH_3)_2CH_2$ from the mixture, i.e., 0:1 ratio), which produced films dominated by surface undulations exhibiting extremely high rms roughness, as expected. Variation in deposition conditions such as temperature, pressure, and compound flux rate did not yield any improvement in the film quality, and all layers produced via this method were defective and rough as determined by XTEM and AFM studies. For example, AFM scans of Ge films with 450 nm thickness grown at 420 °C via pure Ge_2H_6, exhibited an rms roughness of $\sim$30 nm for 5×5 μm^2 areas. In contrast, the roughness for films grown using the 1:15 precursor ratio was found to be 0.2–0.3 nm, which is comparable with atomic step heights on Si. These results collectively indicate that the pseudosurfactant properties of $(GeH_3)_2CH_2$ are enhanced and that the film quality is

(20) Menéndez, J. *Raman Scattering in Materials Science*; Springer: Berlin, 2000.
(21) Cerdeira, F.; Buchenauer, C. J.; Pollak, F. H.; Cardona, M. *Phys. Rev. B* **1972**, *5*, 580.
(22) Anastassakis, E.; Pinczuk, A.; Burstein, E.; Pollak, F. H.; Cardona, M. *Solid State Commun.* **1970**, *8*, 133.
(23) Anastassakis, E.; Cantarero, A.; Cardona, M. *Phys. Rev. B* **1990**, *41*, 7529.
(24) Nakashima, S.; Mitani, T.; Ninomiya, M.; Matsumoto, K. *J. Appl. Phys.* **2006**, *99*, 053512.

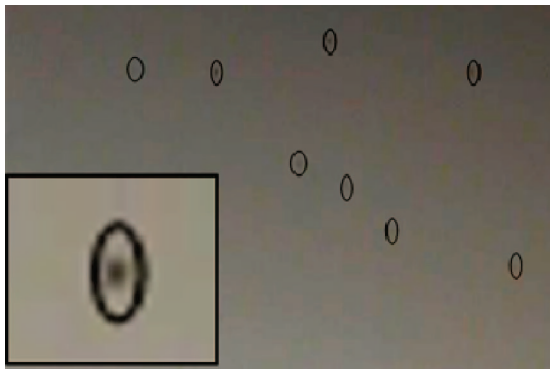

Figure 3. Optical image of the etched Ge surface showing the location of penetrating defects (marked by oval shape ring). Inset illustrates an enlarged site of a typical defect, seen as a dark spot inside the ring.

optimized for reactant ratios close to 1:15 and growth temperatures in the 350–430 °C range.

An etch pit density technique was used to estimate the concentration of threading dislocations in selected samples with thickness close to 0.8 μm. These were etched for typically 200 s at an average rate of ~2 nm/s using a mixture of 700 mL of CH_3COOH, 70 mL of HNO_3, 4 mL of HF, and 270 mg of I_2. The resulting pits were counted from images obtained by an optical microscope (Figure 3). The images showed no dislocations within the first 300–400 nm over areas of 85 × 64 μm^2. At 500 nm, the detectable dislocation densities were found to be below $\sim 1 \times 10^5$ cm^{-2}, and this value increased abruptly toward the interface region. This is consistent with XTEM images that show no threading defects throughout the upper portion of the film but a substantial "pile up" near the interface region. These images also showed atomically flat film surfaces and confirmed the RBS measured thicknesses, which ranged from 0.50 to 2.5 μm in most samples (Figure 4a). The high-resolution micrographs revealed a periodic array of Lomer-type edge dislocations confined to the interface plane (Figure 4b). These likely form in the early stages of growth and provide the necessary strain relief between the highly mismatched substrate and epilayer. Atomic resolution Z-contrast images (not shown) confirmed the presence of edge dislocations and revealed an abrupt transition between the substrate and the epilayer. The interface roughness is less than 1 nm, which appears to be similar to that of the underlying substrate. Electron energy loss nanoanalyis of the interface region indicated no elemental intermixing on the subnanometer scale. The interdiffusion at these low temperatures is therefore suppressed, leading to atomically sharp interfaces. No measurable levels of impurities above the usual background levels were detected by EELS.

XRD reciprocal space maps (RSM) in the vicinity of the (004) and (224) reflections were obtained to precisely determine the in-plane (*a*) and out-of-plane (*c*) lattice constants for the films. The data showed that the Ge films grown by this technique were fully relaxed. This result is consistent with the atomically flat surface morphology and suggests that a layer-by-layer growth mechanism must be in operation in the absence of strain. The relaxation in the samples was so complete that several of the films showed a slight tensile strain upon being cooled to room temperature,

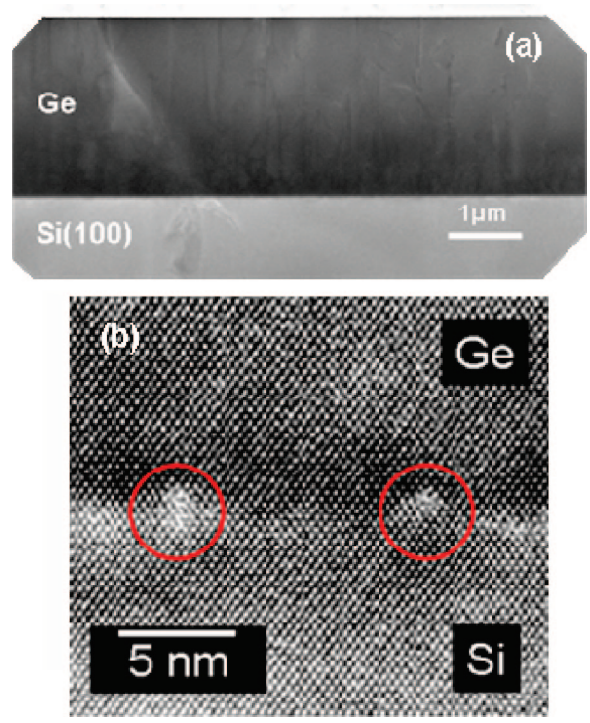

Figure 4. XTEM of a Ge film grown on Si(100) at 420 °C. (a) Phase contrast micrograph showing a 2.5 μm film thickness and a perfectly flat surface. (b) High-resolution image of the heteroepitaxial interface showing the location of Lomer defects (circles).

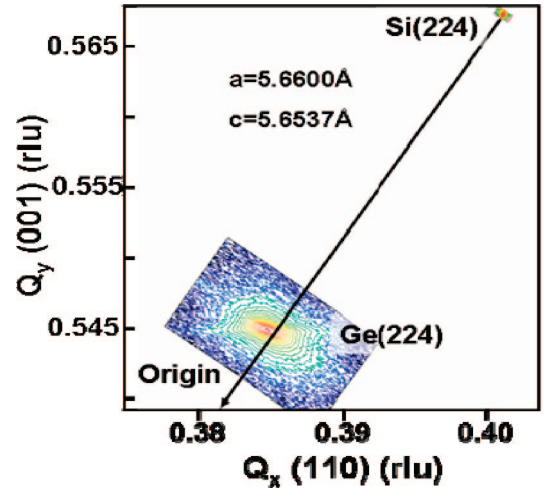

Figure 5. (224) RSM plots of the Ge film shown in Figure 4 and Si substrate. The relaxation line passes near the center of the Ge peak indicating that the material is almost strain-free. This is consistent with the nearly equal values of the *a* plane and *c* lattice constants (shown inset) derived from (224) and (004) Bragg reflections.

presumably because of the thermal mismatch of Ge with the underlying Si substrate. The (224) RSM plot of a sample with ~2.5 μm thickness (Figure 5) shows that the layer possesses a residual tensile strain. The full width at half-maximum of the (004) Bragg reflection for this sample is approximately 400 arcs and the mosaic spread derived from the (224) peak is 250 arcs, indicating slight tilt between grains. Secondary ion mass spectroscopy (SIMS) was also performed on selected samples produced across the entire 350–430 °C temperature regime. Samples grown at 420 °C show a carbon content of $\sim 3 \times 10^{16}$ atoms/cm^3 across the layer, which is below the noise level of the SIMS measure-

ment.[5] The oxygen content in these films was similarly low and dominated by the background level in the SIMS apparatus. We note, however, that at the Ge/Si interface, there is a sharp increase in the C and O concentrations to levels as high as 1×10^{19} cm^{-3}, as indicated by the presence of two distinct peaks corresponding to these elements. Similar features are commonly observed in CVD-grown materials that are typically associated with surface contamination. Figure 12 shows similar interface signatures for the C and O impurities.

To confirm that $(GeH_3)_2CH_2$ does not deposit C during growth, we conducted two control experiments designed to verify that carbon does not migrate to the surface in a typical surfactant fashion. In both cases, an initiation Ge layer of ~250 nm was grown directly on the Si substrate using the 1:15 reactant ratio. A second growth step is then performed in situ immediately after completion of the first layer in order to maintain an uninterrupted growth environment and, more importantly, an unperturbed "as-grown" Ge surface.

In the first experiment, an overlayer of pure Ge was deposited on top of the initiation layer by switching the gas source to pure Ge_2H_6, to eventually produce a thick composite film representative of the two growth modes. XTEM and AFM examinations of the full sample thickness revealed a complete, continuous, and monocrystalline layer with an atomically flat surface (AFM rms $\approx$ 0.4 nm). XTEM also showed that the microstructure throughout the growth transition region is continuous and indistinguishable from the bulk material, indicating that the layer-by-layer growth is uninterrupted in the absence of $(GeH_3)_2CH_2$. SIMS profiles showed a constant Ge content throughout the entire thickness. These results indicate that the "CH_2" fragment of the precursor is continuously eliminated as methane at the growth front and does not accumulate on the Ge surface or become incorporated into the film.

In the second experiment, a pure silicon film was grown on top of the Ge initiation layer via decomposition of $SiH_3SiH_2SiH_3$. This compound incorporates highly reactive SiH_2 groups, allowing the formation of monocrystalline Si at unprecedented low temperatures (420 °C) despite the lower surface energy of the Ge template, which is known to severely hinder such growth in conventional MBE-based processes.

A series of Si films with thicknesses ranging from 2 to 16 nm were deposited using conditions similar to those described above for the Ge growth. High-resolution XTEM was used to characterize the crystallinity, surface morphology, and epitaxial registry of the films. Figure 6 shows the entire Si film thickness (~5 nm) including the interface region with the Ge buffer in high resolution. The microstructure appears to be fully commensurate and the layer surface atomically smooth. Figure 7 shows the Raman spectra of a sample with a 2.5 nm Si film on Ge. The spectrum shows features similar to the Si–Ge and Si–Si Raman peaks in a $Si_{0.5}Ge_{0.5}$ alloy and a high-energy peak that can be assigned to a pure Si layer. This peak is down shifted by about 30 cm^{-1} with respect to the Raman frequency in bulk Si, which according to eq 1 is consistent with a strain level of 4%. A full Raman study of the growth of Si on Ge buffers will be presented elsewhere. This study indicates that the $Si_{0.5}Ge_{0.5}$ alloy is confined to the immediate interface between Ge and Si and that highly strained Si films grow upon subsequent Si deposition (see Figure 7 for a schematic interpretation of the growth).

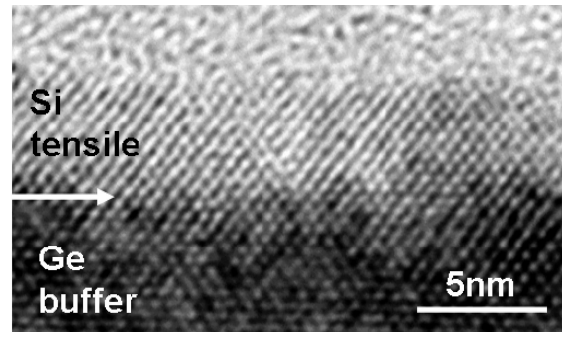

Figure 6. XTEM micrograph of a 5 nm Si film grown on a Ge buffer. The interface is fully epitaxial and the Si epilayer is partially strained (1.5%) because the film has exceeded the critical thickness.

The trisilane deposition directly on our Ge buffers described here establishes proof-of-principle routes for producing continuous, fully pseudomorphic Si layers with tensile-strained structures and atomically flat surfaces. The successful growth of crystalline Si showing a fully commensurate heterointerface unambiguously confirms that the original Ge buffer layer surface must be free of significant carbon-containing impurities originating from decomposition of the organic source. These buffers should also provide an ideal platform for producing Si epilayers with record-high strain states that cannot be accessed via the currently available $Si_{1-x}Ge_x$ ($x \approx 0.20$) counterparts because of their smaller lattice dimensions. Such materials are desirable for high-mobility electronic device applications. The growth of Si directly on Ge would also create new opportunities for the development of Ge-based metal-oxide-semiconductor (MOS) devices.[25] Additionally, thin Si films can act as passivation layers for the growth of high-*k* dielectrics on Ge.[26]

Raman, Photoreflectance, and Photoluminescence of Ge/Si(100). Figure 8 compares the room-temperature Raman spectrum of a 650 nm thick Ge film with that of a reference Ge bulk substrate, obtained with 532 nm excitation. For this wavelength, the penetration depth of light in Ge is approximately 18 nm (so that the Raman signal originates mainly from the first 9 nm). According to the X-ray data, the film strain is relaxed. Because, as mentioned above, the only allowed first-order Raman peak corresponds to the highest-frequency vibration in the perfect crystal, the presence of defects should shift and broaden the line toward lower Raman shifts. In our case, the film Raman spectrum is very similar to that of the Ge bulk substrate, confirming the high quality of our film. A very small frequency upshift is observed, which we assign to a residual amount of compressive strain. Using eq 1, we estimate that this

(25) Shang, H.; Frank, M. M.; Gusev, E. P.; Chu, J. O.; Bedell, S. W.; Guarini, K. W.; Ieong, M. *IBM J. Res. Dev.* **2006**, *50*, 377.
(26) De Jaeger, B.; Bonzom, R.; Leys, F.; Richard, O.; Steenbergen, J. V.; Winderickx, G.; Moorhem, E. V.; Raskin, G.; Letertre, F.; Billon, T.; Meuris, M.; Heyns, M. *Microelectron. Eng.* **2005**, *80*, 26.

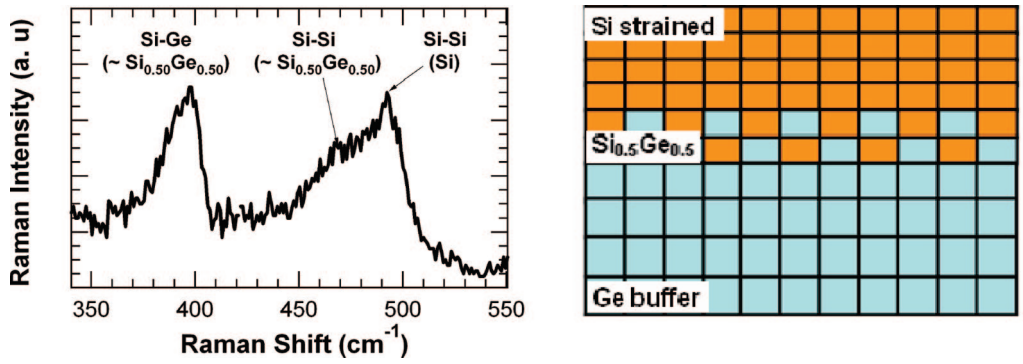

Figure 7. (Left) Raman spectra showing the Ge–Si and Si–Si peaks of a fully coherent $Si/Si_{0.50}Ge_{0.50}$structure. The tensile strained Si overlayer with thickness ~2.0 nm is grown on a Ge buffer via a self-assembled subnanometer thick $\sim Si_{0.50}Ge_{0.50}$ interface layer. (Right) Schematic showing a fully coherent heterostructure comprised of the cubic Ge buffer (blue squares), the tetragonally distorted SiGe interface (blue and gold),and the tensile strained Si overlayer (gold).

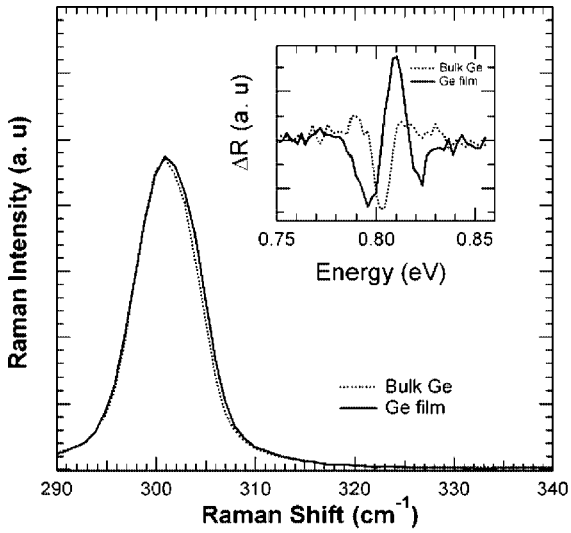

Figure 8. Raman spectrum of a 650 nm Ge film grown on Si (solid line) compared with that of a bulk Ge substrate (dotted line). The inset shows room-temperature photoreflectance spectra for both samples, using the same convention for the lines. The measured energy range corresponds to the direct gap of Ge.

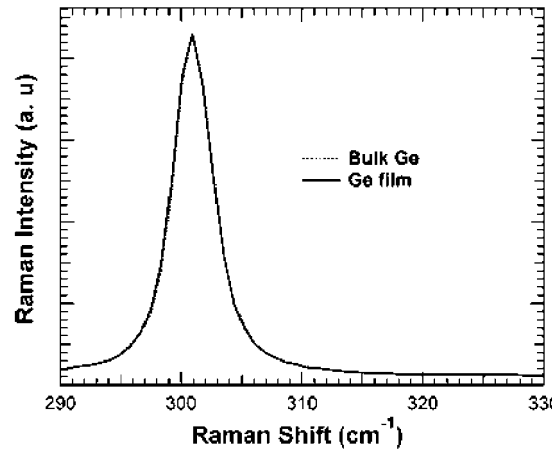

Figure 9. Raman spectrum of a 500 nm Ge film on Si (solid line) compared to that of bulk Ge (dotted line). The overlap between the two spectra is perfect.

compressive strain is 0.04%. It is apparent from Figure 8 that this is close to the detection limit of the Raman technique and within the error of the X-ray measurements. The inset in Figure 8 shows room-temperature photoreflectance results in the spectral region corresponding to the lowest direct gap E_0. We fit the spectra with standard expressions for critical point features, and for the reference Ge substrate we find $E_0 = 0.803(1)$ eV. For the Ge film, the transition is slightly shifted to 0.806(1) eV, and the broadening parameter is virtually identical to that of bulk Ge. Interestingly, if we use standard deformation potential theory to calculate the strain shift of the band gap for 0.04% compressive strain, we find that the heavy-hole band gap increases by 3 meV, in agreement with the observed shift. Thus the photoreflectance measurement is consistent with the Raman result and both confirm the high quality of the Ge-film and the very small magnitude of the residual strain. Moreover, the example discussed in Figure 8 represents in a certain sense a "worst-case" scenario: in other samples, we find absolutely no discernible difference between the Raman spectrum of the Ge film and that of the Ge substrate. In Figure 9, we show data for one such sample. Its Raman spectrum essentially overlaps the Raman spectrum of bulk Ge. This sample also shows a weak but clearly observable photoluminescence peak upon excitation with 250 mW of 488 nm light. The peak maximum at 0.745 eV is very close to the position of the indirect edge in pure Ge.

Selective Growth in Prototype Device Structures. Selective growth was conducted using a wafer provided by ASM America (Phoenix AZ), incorporating various device architectures including simple transistor structures and various patterns masked by amorphous nitride and oxide thin layers. The wafer was cleaved to produce substrates with suitable dimensions to fit the sample stage of the growth chamber. These were rinsed with methanol and then dipped in HF to remove the thin oxide covering the bare Si surface on the wafer while preserving the nitride masked areas essentially intact. The resulting samples were inserted into the reactor and flashed briefly for 1 s at 1000 °C to remove any residual contamination from the surface. The Ge films were grown for 30 min at 380 °C and 5×10^{-5} Torr using the 1:15 mixture of $(GeH_3)_2CH_2/Ge_2H_6$, which was routinely employed for deposition directly on Si. The as-deposited samples exhibited an appearance essentially identical to that of the underlying patterned wafer material. Optical microscopy revealed that the appearance of the nitride/oxide masked regions was unchanged, whereas the coloration of the Si-based areas was changed from a metallic gray, typical of Si,

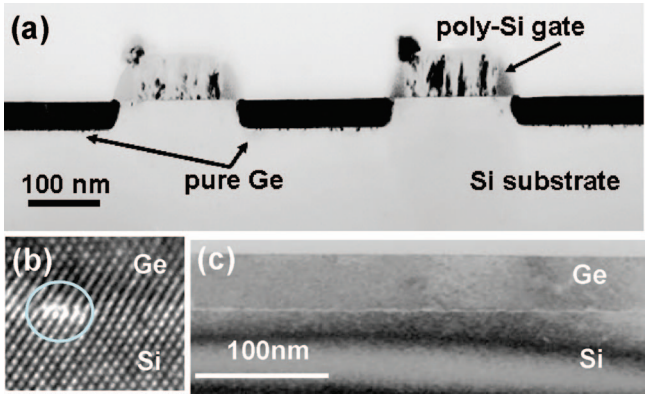

Figure 10. (a) Ge trenches grown selectively in the "source" and "drain" areas of a device. Note the absence of any deposition on nitride spacers or on the polysilicon gate hardmask. (b) Micrograph of the Ge/Si interface showing the location of an edge dislocation (circle). (c) XTEM image illustrating the formation of smooth layers devoid of threading defects on Si-exposed areas within the complex wafer structure.

to a light brownish hue, indicating that selective deposition had occurred. A comprehensive characterization of the wafers by RBS, XRD, AFM, XTEM, and EDX (energy-dispersive X-ray) revealed the presence of atomically flat Ge films with single-crystalline and fully relaxed microstructures throughout the sample.

The film nominal thickness was estimated by the random RBS spectra to be in the 45–50 nm range, yielding an average growth rate of ~2 nm/min. The channeled spectra indicated that the material was highly aligned and commensurate with the underlying substrate. The XTEM micrograph in Figure 10 confirms that the deposition of Ge occurred selectively in the "source" and "drain" areas of the devices and not on the nitride spacers or on the polysilicon gate hardmask. High-resolution images of the interface showed a perfect epitaxial registry between the Ge film and the surrounding Si wafer structure with typical edge dislocations accommodating the strain differential between the materials. The micrographs clearly demonstrated that the Ge deposited conformably on the sidewalls and bottom of the trench portion of the device feature entirely filling the drain/source region. The perfectly flat surface morphology of the Ge layer, as shown in the AFM and XTEM images (Figure 10c), is consistent with a layer-by-layer growth mode. We note that the polygermanium nodule that is observed at the corner of the spacer and the gate hardmask (Figure 10a) is where the wet etch broke through the hardmask, enabling germanium nucleation from the underlying polysilicon. The occurrence of these nodules can be controlled by further refining the HF-based etching process. Future experiments will focus on perfecting the sample preparation and growth conditions to produce relaxed and strained materials on large area substrates to enable measurements of the electrical and optical properties on entire arrays of device structures. The seamless and fully conformal growth of strained free Ge in the recessed source/drain regions might provide a route to extending the use of group IV materials to induce compressive strain in the silicon channel for increased hole mobility applications.

Strain-Free Depositions via GeH_3CH_3. The GeH_3CH_3, analog of $(GeH_3)_2CH_2$, was also explored as a potentially practical source to grow Ge films on Si at low temperatures between 360 and 420 °C. The experiments were performed at constant deposition pressure of 5×10^{-5} Torr using suitable mixtures of the compound with Ge_2H_6 at molar concentration ranging mostly from 1:5 to 1:15. The substrate preparation and sample handling procedures were essentially identical to those described above for the experiments involving $(GeH_3)_2CH_2$.

Preliminary depositions using a dilute GeH_3CH_3:Ge_2H_6 reactant ratio of 1:20 produced crystalline but visibly rough layers exhibiting a cloudy surface appearance. AFM indicated an rms roughness of 8–9 nm and revealed a surface morphology dominated by a network of two-dimensional terraces with variable size, shape, and orientation. This is in stark contrast to the usual three-dimensional islands or surface ripples typically observed in conventional Ge growth at this temperature. To further improve the film morphology, we increased the reactant molar ratio to the 1:15 and performed a series of depositions at 360, 380, 400, and 420 °C using this mixture. The resultant films displayed a smooth appearance indistinguishable from that of the underlying substrate, indicating that the samples were flat and crystalline.

Characterizations by RBS including ion channeling indicated highly aligned layers in perfect commensuration with the substrate. In most samples, the ratio of the channeled versus the random peak heights (χ_{min}), which measures the degree of crystallinity, decreases from 10% at the interface to 4% across the layer, indicating a dramatic reduction in dislocation density (the 4% value represents the theoretical limit in pure Si). RBS carbon resonance experiments were used to confirm the absence of carbon impurities within the bulk of the material. The corresponding depth profiles using a series of ion beam energies with variable penetration depths did not reveal any measurable carbon contamination within the uncertainty of the measurement (less than 0.5 at %). The RBS derived thicknesses for the Ge/Si(100) layers varied from 400 to 600 nm with increasing temperature from 360 to 420 °C, with a concomitant increase in growth rate from 5 to 10 nm/min, respectively.

Among these samples, the AFM examinations of films deposited at 400 and 420 °C revealed flat surface morphology with an rms roughness of 0.2 nm. However, the AFM images also revealed that approximately 5% of the sample surface was covered by an array of perfectly rectangular nanoscale depressions (Figure 11). XTEM micrographs indicate that their lateral and vertical dimensions are 100–150 and 10–15 nm, respectively, corroborating the surface patterns and morphologies observed by AFM. In addition, the horizontal surface and vertical edges were perfectly planar and approximately orthogonal, indicating that these depressions have a parallelepiped matchboxlike shape. The low-magnification XTEM images also revealed an average layer thickness of 400 nm and an overall flat surface morphology interrupted by the occasional presence of the depressions in these samples. Finally, we note that lowering the sample growth temperature into the 360–400 °C range produced samples in which the density of these depressions could be reduced to an arbitrarily low value, but not entirely eliminated.

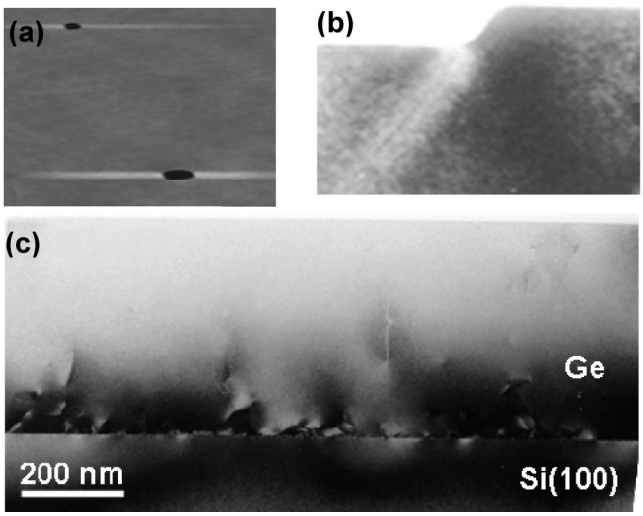

Figure 11. AFM and XTEM images of a Ge sample containing surface depressions. (a) AFM image (1 μm × 0.8 μm) in the vicinity of two representative "match box" depressions. (b) Diffraction contrast micrograph showing the cross-sectional morphology for one of these features, including one vertical edge and a section of the horizontal bottom surface.(c) XTEM image of the sample showing an atomically smooth layer devoid of threading defects penetrating to the surface within the field of view.

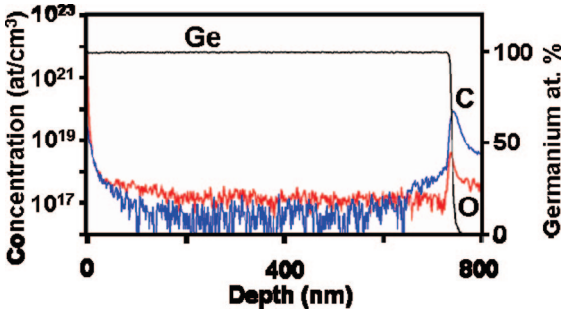

Figure 12. SIMS profile of an ~700 nm Ge film deposited using GeH_3CH_3/Ge_2H_6 in a 1:10 ratio at 360 °C. The data show no measurable C contamination across the layer. Impurity level C and O peaks are observed at the sharp Ge/Si interface.

Accordingly, we further increased the concentration of GeH_3CH_3 beyond the 1:15 ratio to determine its effect on the surface properties and film growth rates. Depositions using 1:10 mixtures at temperatures near 420 °C produced thick films exhibiting substantial concentrations of the matchbox depressions. However, for this reactant stoichiometry, lowering the temperature to 360 °C yielded perfectly flat films completely devoid of these features. The growth rate in this case (GeH_3CH_3at 360 °C) is 5 nm/min, which is essentially identical to that obtained from the deposition of $(GeH_3)_2CH_2$ at 420 °C. Thus, the GeH_3CH_3 compound is the best candidate to date for viable low temperature Ge growth compatible with selective area applications. Depositions using 1:5 mixtures produced comparable surface morphologies; however, the growth rates were significantly reduced to levels below 3 nm/min. In the limiting case of using the pure GeH_3CH_3 compound as the sole reactant (1:0 molar ratio), we obtained negligible film growth. This indicates that the Ge films in these reactions must be generated by the facile surface dissociation of the highly reactive $(GeH_3)_2$ species and the role of the organic analog is to catalyze or facilitate layer-by-layer growth. To confirm the absence of carbon in the bulk of the film, we analyzed selected samples by SIMS compositional profiles. The data showed that all materials were essentially free of carbon and displayed very similar C and O profiles to those observed previously in the related growth studies using the $(GeH_3)_2CH_2$ compound.

Figure 12 shows a typical profile for a sample deposited at 360 °C using a 1:10 ratio of GeH_3CH_3 in Ge_2H_6. Note that the carbon content remains below the detection limit (~1×10^{16} at/cm^3) throughout the entire thickness of the sample, with a sharp rise to a value $<10^{20}$ at/cm^3 at the interface. The C and O profiles found here are also essentially identical to those observed in our previous growth studies using the $(GeH_3)_2CH_2$ compound.[5] These levels are in fact quite typical for CVD materials grown under these conditions. Thus, the carbon enhancement near the interface is not likely associated with the reactivity of the particular precursor employed.

It is interesting to note that 30 nm thick Ge:C films have been demonstrated in high-temperature (<450 °C) depositions of GeH_3CH_3 by UHV-CVD. In this case, the intentional incorporation of carbon at the 1% level purportedly produces surface roughness of ~3 Å and low defect densities of 3×10^5 cm^{-2}.[27] SIMS profiles showed that the carbon segregates toward upper/lower portion of the films near the surface/interface regions. The layers are slightly compressed with a net relaxation of ~78% and are typically too thin for optical applications but could prove useful for Ge channel MOSFETs.[28] Our deposition experiments using GeH_3CH_3 were conducted on a single-stage wafer configuration at significantly lower temperatures (360 °C), which precluded any of the side reactions that might lead to carbon contamination.

Calculations of Surface Energetics. It is well-known that under the temperature/pressure parameters described above, Ge film growth using pure digermane proceeds via the classic Stranski–Krastanov process by formation and coalescence of three-dimensional islands, ultimately leading to the creation of rough films dominated by surface undulations. Collectively, our experiments demonstrate that small concentrations of the $(GeH_3)_2CH_2$, GeH_3CH_3 organic additives can profoundly alter this conventional film growth mechanism, leading to the assembly of flat, strain-free films with record-low defect densities. The highest-quality films are obtained for optimum concentration ratios of 1:10 for GeH_3CH_3 and 1:15 for $(GeH_3)_2CH_2$ in digermane.

To elucidate how the organic derivatives influence the classic digermane growth process so dramatically, we use fundamental bond energies as a guide to develop plausible surface reaction mechanisms. We proceed with the following assumptions: (i) the low temperatures and pressures (1×10^{-5} Torr) preclude gas-phase reactions among the various deposition species (GeH_3CH_3 or $(GeH_3)_2CH_2$, and Ge_2H_6); (ii) the strong C–H bonds prevent facile degradation of the GeH_3–CH_3 or GeH_3–CH_2–GeH_3 precursors in this temperature range; (iii) the precursors react at the growth front by

(27) Kelly, D. Q.; Wiedmann, I.; Donnelly, J. P.; Joshi, S. V.; Dey, S.; Banerjee, S. K.; Garcia-Gutierrez, D. I.; Jose-Yacaman, M. *Appl. Phys. Lett.* **2006**, *88*, 152101.
(28) Kelly, D. Q.; Wiedmann, I.; Garcia-Gutierrez, D. I.; Jose-Yacaman, M.; Banerjee, S. K. *Semicond. Sci. Technol.* **2007**, *22*, S204.

forming Ge–Ge bonds with the underlying surface. This implies that they do not simply physisorb to act as kinetic dilutants or nonbonded surface diffusion barriers but participate in the growth of the film via the deposition of their GeH_3 groups.

Simple gas kinetics dictates that the arrival rate of gaseous species at a surface is given by the classic formula $J = P/\sqrt{2\pi m k_B T}$, where P = pressure, T = temperature, m = molecular mass, and k_B is Boltzmann's constant. At a typical temperature of 360 °C and $P = 5 \times 10^{-5}$ Torr, this model gives arrival rates of 70, 60, and 50 molecules nm^{-2} s^{-1} for the pure, undiluted $(GeH_3)_2CH_2$, Ge_2H_6 ,and GeH_3CH_3 compounds, respectively. For the specific case of a 1:10 GeH_3CH_3:Ge_2H_6 mixture, the corresponding flux ratio is also 1:10, which indicates that a significant number of GeH_3CH_3 molecules arrive at any given time. Using a sticking coefficient $\sigma = 0.05$, which is a typical value of Ge_2H_6 on Si surfaces at these conditions,[29] we obtain a growth rate $R = \Omega J \sigma$ equal to ~4–5 nm/min (where $\Omega = 22.7$ Å^3 is the volume per Ge atom in the film). The R value in this case is remarkably close to that of the growth rates obtained in the experiments described previously. However, the predicted growth rate using the above formula decreases with increasing temperature, in contradiction with our observation that the growth rates increase slightly in going to 420 °C. This clearly indicates that higher reaction rates at 420 °C must contribute to the rate of growth.

In the case of deposition of pure GeH_3CH_3 at 360 °C, the lack of a measurable growth rate in spite of the significant impingement flux indicates that a certain minimum concentration of digermane is required at the growth front to activate the release of methane, otherwise the accumulation of organic derivatives might lead to surface passivation and termination of growth. In a related control experiment using $(GeH_3)_2CH_2$ at a concentration ratio of 1:2–1:5, no measurable growth was observed, corroborating the notion that excess organic derivatives could lead to "surface poisoning". This assumption precludes a mechanism based on a simple physisorption model and also suggests that the molecules react with the growth surface in the presence of digermane.

Accordingly, we assume that in both cases the CH_3GeH_3 and $(GeH_3)_2CH_2$ react and bond to the surface via the Ge atoms of the GeH_3 ligands. This likely involves the formation of surface intermediate species comprising $–GeH_2–CH_3$ and $–GeH_2–CH_2–GeH_2–$ complexes, respectively, which remain intact at the low growth operating temperatures of 360–420 °C because of the strong C–H and Ge–C bonds (see Figure 13). These intermediates are envisioned to be analogous in both function and size to the traditional Sb or As surfactant atoms used to produce flat Ge films grown on mismatched substrates. They promote wetting and suppress diffusion of the Ge adatoms, thereby enforcing the formation of a flat surface morphology. In our experiments, the surface-bonded $–GeH_2–CH_3$ or $GeH_2–CH_2–GeH_2–$ intermediates also promote flat layer growth by effectively serving as site holders

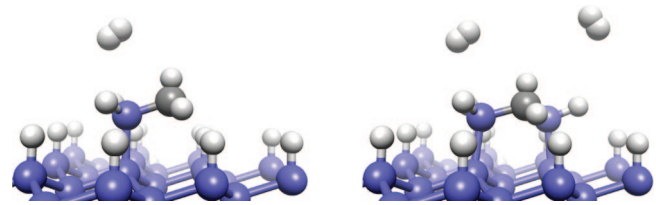

Figure 13. Surface intermediates formed by the reaction of the GeH_3CH_3 and $(GeH_3)_2CH_2$ with the hydrogenated film surface. Blue, grey, and white spheres represent Ge, C, and H atoms, respectively.

Table 1. Calculated Bond Enthalpies (kcal/mol) for Bonds between H, C, and Ge (available experimental values are in parentheses)

	H	C	Ge
H	110 (104)	105 (99)	73 (69)
C		80 (83)	56 (58)
Ge			38

that facilitate the organized assembly of smooth films and are continuously replenished by the incident molecular precursor flux. Unlike conventional surfactants, which are admitted at the onset of growth and then recycled, these organic species react and desorb CH_4, which is generated via Ge–C cleavage induced by incoming Ge_2H_6 reactant molecules or by H_2 reaction byproducts. Thus, as the molar concentration of organics is increased from an optimal value to the lowest 1:0 limit, the accumulation of unreacted intermediates saturates the available reaction sites, preventing further Ge growth.

A similar mechanism is also operative in CVD of SiGe films on Si, where adsorbed H is well-known to suppress diffusion of GeH_x and thus promote layer-by-layer growth. In our system, the heavier and chemically robust organic units provide an effective diffusion barrier on the time scale of H_2 desorption. Furthermore, the low temperature reduces the diffusion rate of mobile surface species such as H and Ge adatoms. Although the solubility of C into Ge is negligible, its incorporation into the lattice as a metastable substitutional impurity is nevertheless possible at these low temperatures. However, this requires breaking of multiple C–H bonds, which is unlikely on thermodynamic grounds under these conditions (350–420 °C, 1×10^{-5} Torr pressure).

Ultimately, the elimination of the CH_2 and CH_3 groups as CH_4 is the dominant driving force in this process. This can be quantified using bond enthalpies, which allow approximate calculation of the various plausible surface reactions involving these compounds on H-terminated Ge surfaces that mimic the local growth environment. Although some of the required bond enthalpies are known, the values involving Ge are not fully available.[30] For this purpose and internal consistency in our estimates, we have conducted ab initio calculations to determine the bond enthalpies involving H, C, and Ge binary combinations. Using the B3LYP functional at the N311++(2d,2p) level of theory, we obtain the values listed in Table 1.

We consider three mechanisms for the reaction of the GeH_3CH_3 molecules with the Ge growth surface as shown

(29) Schwarz-Selinger, T.; Foo, Y. L.; Cahill, D. G.; Greene, J. E. *Phys. Rev. B* **2002**, *65*, 125317.

(30) Bills, J. L.; Cotton, F. A. *J. Phys. Chem.* **1964**, *68*, 806.

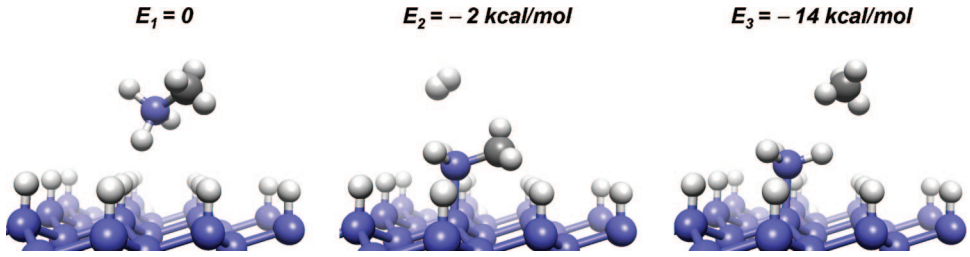

Figure 14. Proposed two-step reaction process involving the evolution of methane and the adsorption of germyl (third scenario described in the text).

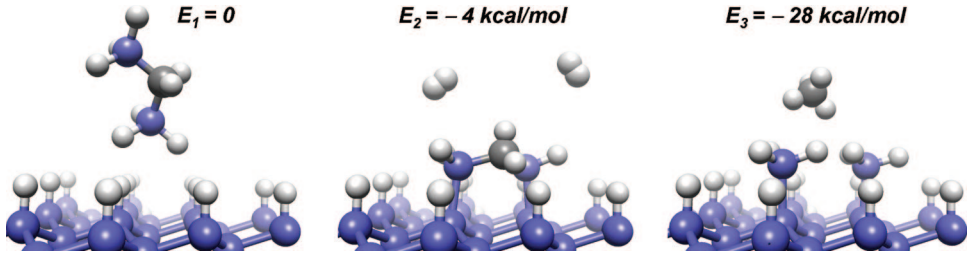

Figure 15. Proposed two-step reaction process involving adsorption of GeH_3-CH_2-GeH_3 compound via evolution of methane.

Figure 14. In reaction 1 shown below (Rx1), the molecule decomposes via breaking the Ge–C bond, to adsorb the methyl (CH_3) and the germyl (GeH_3) fragments onto the Ge–H surface. The corresponding reaction energy obtained from the bond enthalpies equals $\Delta H = -2$ kcal/mol, assuming that the entropy change for the process is zero.

$$GeH_3CH_3(g) + 2Ge(ads)\text{–}H \rightarrow Ge(ads)\text{–}CH_3 + Ge(ads)\text{–}GeH_3 + H_2(g) \quad \Delta H = -2 \text{ kcal/mol} \quad \text{(Rx1)}$$

The second reaction can be viewed as a two-step process involving the formation of a surface intermediate complex in which the $–CH_2GeH_3$ ligand is bonded to the surface via the CH_2 functionality (Rx2a)

$$GeH_3CH_3(g) + Ge(ads)\text{–}H \rightarrow Ge(ads)\text{–}CH_2GeH_3 + H_2(g) \quad \Delta H = +12 \text{ kcal/mol} \quad \text{(Rx2a)}$$

The reaction energy of this step is +12 kcal/mol (as shown below), indicating that the formation of Ge–C bonds on the surface is unfavorable. In the second step, the complex decomposes with the release of germane and the binding of a methyl group (Rx2b)

$$Ge(ads)\text{–}CH_2GeH_3 + H_2(g) \rightarrow Ge(ads)\text{–}CH_3 + GeH_4(g) \quad \Delta H = -12 \text{ kcal/mol} \quad \text{(Rx2b)}$$

The net reaction energy is thus zero because the same number and type of bonds are broken and formed (Rx2a + Rx2b)

$$GeH_3CH_3(g) + Ge(surface)\text{–}H \rightarrow Ge(surface)\text{–}CH_3 + GeH_4(g) \quad \Delta H = 0 \text{ kcal/mol} \quad \text{(Rx2a+Rx2b)}$$

The third reaction involves a two step mechanism in which the precursor is adsorbed via the $–GeH_2$ functionality, with a reaction energy of −2 kcal/mol (compared with +12 kcal/mol in the second reaction scenario above). Here, however, the subsequent decomposition step releasing the extremely robust methane molecule and binding the germyl group onto the Ge surface evolves an additional −12 kcal/mol. As expected, this is the most favorable reaction, with a net overall energy of −14 kcal/mol (Rx3)

$$GeH_3CH_3(g) + Ge(surface)\text{–}H \rightarrow Ge(surface)\text{–}GeH_3 + CH_4(g) \quad \Delta H = -14 \text{ kcal/mol} \quad \text{(Rx3)}$$

From a chemical point of view the release of methane thus represents the dominant driving force in the growth reactions involving the CH_3–GeH_3 precursor.

For the reaction GeH_3–CH_2–GeH_3 compound, we consider only two plausible reaction schemes for the incoming molecules with the Ge growth surface (Figure 15). The first proceeds with the attachment of a single germyl group to the surface, whereas the second involves simultaneous binding of both germyl end members to the surface. The third possibility, in which the molecules binds to the surface via the central $–CH_2–$, is highly unfavorable on energetic grounds and is not considered.

In the first case, the $–GeH_3$ ligand of GeH_3–CH_2–GeH_3 attaches to the surface via a single proton transfer and releases GeH_3CH_3. This process is dominated by the breaking of one of the Ge–C bonds, leading to a net energy change of +24 kcal/mol (note that H_2 is not evolved in this process). Because the associated entropy change is small (unimolecular reaction) the process is dominated by the enthalpy change, and is thus highly endothermic. If we consider that the GeH_3CH_3 then reacts with the surface via methane abstraction as described by Rx3 (−14 kcal/mol), the net energy for the entire deposition reaction is

$$GeH_3CH_3 + Ge(surface)\text{–}H \rightarrow Ge(ads)\text{–}GeH_3 + GeH_3CH_3(g) \rightarrow 2Ge(ads)\text{–}GeH_3 + CH_4(gas) \quad \Delta H = +10 \text{ kcal/mol} \quad \text{(Rx4)}$$

On the basis of this simple analysis, growth via this decomposition route is thus unfavorable.

In the case where both GeH_3 end members of GeH_3–CH_2–GeH_3 bind to the surface, as shown in Figure

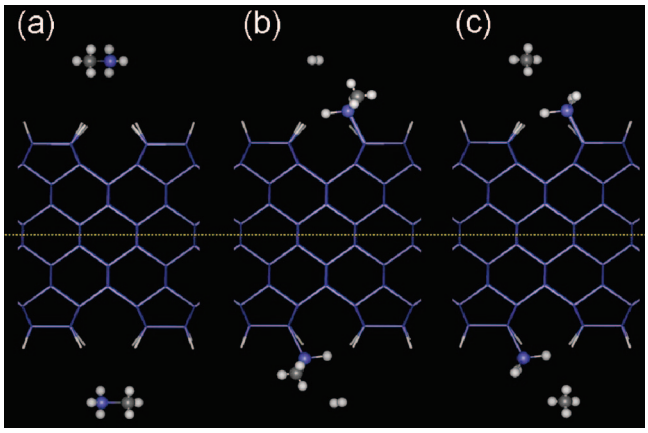

Figure 16. Supercell geometries used for the calculation of adsorption energies of GeH_3CH_3 on a hydrogenated (2 × 1) Ge(001) surface. Reactions R × 1, R × 2, and R × 3 are depicted in panels a–c, respectively. The dotted line represents the center of the slab, where bulk conditions prevail.

15, we obtain a strained methylene-bridged –GeH_2–CH_2–GeH_2– complex via the liberation of 2 H_2 molecules and an energy change of −4 kcal/mol. In the next step, methane is released with a corresponding reaction energy of −24 kcal/mol. The net reaction energy for this entire process is therefore −28 or −14 kcal/mol per –GeH_3 adsorbed. This is therefore a highly favorable route comparable to that described by Rx3. Note that the significant bond strain associated with the methylene-bridged –GeH_2–CH_2–GeH_2– complex is due to the small size of the carbon atoms compared to Ge and likely promotes the facile removal of the CH_2 as methane.

To corroborate the surface reaction energies obtained from bond enthalpies, we carried out a series of large-scale control calculations for the GeH_3CH_3 on a proton-terminated Ge(001) surface using state-of-the-art electronic structure simulations at the LDA level. A parallel implementation of the VASP[32] code was used to obtain all of the optimized structures and electronic properties. The hydrogen-terminated Ge(001) substrate was represented by a 180 atom slab with a thickness sufficient to ensure complete bulk behavior in the interior, and a large supercell dimension of 80 Å normal to the surface was used to minimize coupling between periodic slab replicas. To preclude the development of long-range fields, we adopted configurations with symmetrical molecular adsorption geometries on both sides of the slab, as shown in Figure 16. Core electrons were replaced by ultrasoft pseudoptentials, and the remaining valence electrons were expanded in a plane-wave basis using an energy cutoff of 500 eV and a single *k*-point sampling at Γ. Unlike our simple bond enthalpy models above, the large-scale slab representations adopted here implicitly incorporate surface relaxation effects induced by the adsorbing molecules. This may be particularly important in the case of $(GeH_3)_2CH_2$ adsoption because the methylene-bridged –GeH_2–CH_2–GeH_2– complex may transfer strain from the complex to the surface. Our detailed simulations confirm that the adsorbed complex bears the majority of the distortion, whereas the surrounding Ge substrate remains essentially unperturbed. Accordingly, in this case, the simple addition of bond enthalpies is fairly quantitative. In fact, our calculated energies confirm the general trends predicted by the bond enthalpy calculations for all cases considered. For example, in reaction Rx2, where the methyl is adsorbed and GeH_4 is released, we find an energy change of −1 kcal/mol for the overall process. This is close to zero, as expected on the basis of bond formation/breakage discussed above. Similarly, the most energetic reaction involving the release of methane and the binding of a GeH_3 occurs with an energy difference of −17 kcal/mol, which is very similar to the value −14 kcal/mol predicted using bond enthalpies. The main origin of this energy difference is the use of the LDA in the slab calculations and B3LYP treatment in the bond enthalpies. An ∼20–30% overbinding is typical of LDA with respect to B3LYP, suggesting that bond enthalpies in Table 1 can be used as a reasonable quantitative tool for characterizing the simple surface reactions in our H–C–Ge system.

Tensile-Strained Ge Growth. We have also exploited the unique growth properties of the $(GeH_3)_2CH_2/Ge_2H_6$ formulations to produce tensile-strained Ge films on $Ge_{1-y}Sn_y$ buffered Si substrates, for the first time. The strain state in this case can be systematically manipulated by varying the thickness and composition of the underlying $Ge_{1-y}Sn_y$ template, which possesses the required lattice parameters larger than that of Ge. The $Ge_{1-y}Sn_y$ ($y = 0.02$–0.04) buffer layers in these experiments were grown as described previously.[6] In all cases, a postgrowth rapid thermal annealing step was performed to ensure that the buffers were fully relaxed. Films with compositions of 2 and 4% Sn were heated to temperatures of 700 and 600 °C for 10 s, respectively. Subsequent growth was then conduced using a 1:15 mixture of $(GeH_3)_2CH_2$ in Ge_2H_6. The substrates were sonicated in methanol, inserted into the UHV reactor via a load lock, and then heated on the sample holder for 1 h at 250 °C to desorb any volatile surface contaminants until the chamber pressure was restored to the base value of 1×10^{-10} Torr. Under these conditions, we find that the $Ge_{1-y}Sn_y$ surfaces exhibit the typical (2 × 1) to (1 × 2) reconstruction, indicating a well-ordered crystallographic state suitable for subsequent heteroepitaxial growth. The temperature was then increased to 360–380 °C and the reactant gases were admitted at a final pressure of 5×10^{-5} Torr to commence film growth. Typical growth times from 30 to 60 min yielded films of thickness in the range 30–60 nm, respectively, at a fixed growth temperature of 360 °C. Under these conditions, the growth is observed to proceed via nucleation of nanoscale atomically flat mesas, which gradually coalesce to produce continuous films with planar surfaces as evidenced by AFM characterizations. At higher growth temperatures of 380 °C, we observe a significant increase in growth rate and a surface morphology consisting of two-dimensional tiling formations based on rectangular mesas with variable shape and size. On the length scale of the mesas (∼1 μm) the film surface is atomically flat; however, on the scale of 2–5 μm the surface roughness is higher because of the presence of vertical steps between the mesas.

The films $Ge/Ge_{1-y}Sn_y$ were also characterized by RBS, XRD, and XTEM to establish their composition, thickness, crystallographic properties, strain state, and morphology. The RBS random and aligned spectra revealed a two-layer

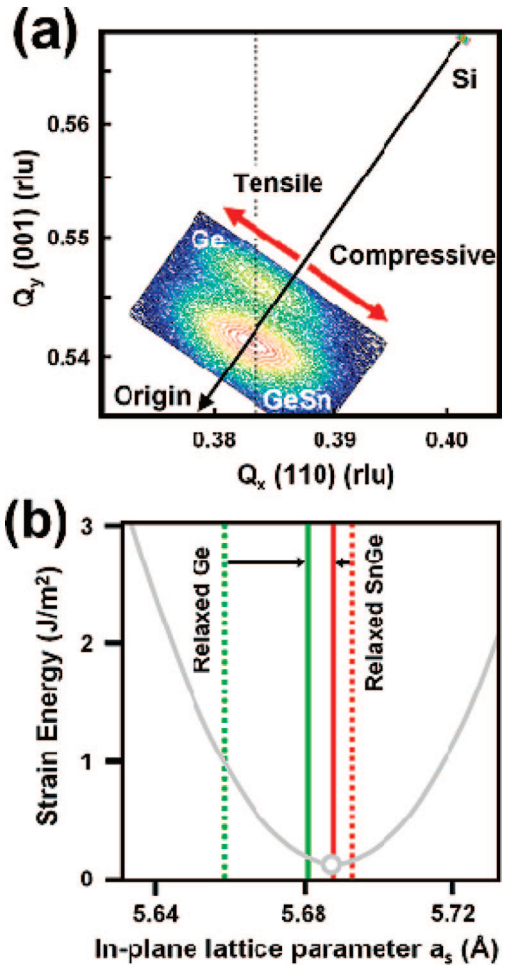

Figure 17. (a) (224) reciprocal space maps of the Ge/$Ge_{0.965}Sn_{0.035}$ stack relative to the Si substrate peak. The Ge peak falls above the relaxation line connecting Si and the origin, indicating tensile strain. The peak maxima for Ge and GeSn are perfectly aligned (dotted line), indicating identical in-plane dimensions. (b) Strain equilibration in the Ge/$Ge_{0.965}Sn_{0.035}$ bilayer. The relaxed Ge and GeSn in-plane lattice parameters (dotted lines) are shifted (arrows) towards a common minimum (open circle) to minimize the combined strain energy. Note that the buffer layer is only slightly compressed.

heterostructure perfectly aligned with the Si substrate, as evidenced by the extremely low χ_{min} value of 10% within the Ge layer (χ_{min} is the ratio of the aligned to random RBS peak heights). The strain state of the films was investigated by recording XRD line scans and reciprocal space maps for the symmetric (004) and asymmetric (224) Bragg reflections. In each case, the data were referenced to the corresponding reflections of the Si wafer. Figure 17a shows the (224) spectra of a representative sample with composition Ge/$Ge_{0.965}Sn_{0.035}$, and epilayer/buffer thicknesses of ~60/230 nm. The plots show that the much thicker buffer in this heterostructure is essentially relaxed and nearly cubic ($a_{\parallel,GeSn}$ = 5.6872 Å, $a_{\perp,GeSn}$ = 5.6955 Å). This is further confirmed by the proximity of the GeSn peak maximum to the relaxation line connecting the corresponding Si (224) peak to the origin of the plot. The plots also show a near perfect vertical alignment of the Ge and GeSn (224) peaks indicating a fully coherent stack, as shown by the dotted line in Figure 17a. Note the considerable vertical offset of the Ge peak with respect to the relaxation line, indicating a significant tensile strain that is manifested as a tetragonal distortion that accommodates the large lattice mismatch with the buffer. The ideal strain equilibration behavior[31] of the Ge/$Ge_{0.965}Sn_{0.035}$ sample is plotted in Figure 17b, which shows that most of the strain energy minimization is accounted for by the expansion of the Ge epilayer in the *a*–*b* plane. This indicates that for thick (>200 nm) buffers,very little change in the dimensions of the buffer is expected.

To derive the precise values of the in-plane ($\epsilon_\parallel$) and perpendicular ($\epsilon_\perp$) strain values,we conducted a quantitative analysis of the XRD data assuming that the epitaxial Ge films adopt a purely tetragonal distortion relative to their unstrained cubic form, in which $\epsilon_\parallel = (a_\parallel - a_0)/a_0$ and $\epsilon_\perp = (a_\perp - a_0)/a_0$ (where $a_\parallel$, $a_\perp$, and a_0 are the measured in-plane, vertical, and relaxed lattice constants, respectively). The two strains are related by $\epsilon_\perp = -2C_{12}/C_{11}\,\epsilon_\parallel$, which we can write $\epsilon_\perp = -\xi\epsilon_\parallel$, with $\xi = 2C_{12}/C_{11}$ (where C_{12} and C_{11} are the elastic constants). The strain relation can be inverted to obtain the unstrained lattice constant $a_0 = (a_\perp + \xi a_\parallel)/(1 + \xi)$, the $\epsilon_\parallel = (a_\parallel - a_\perp)/(a_\perp + \xi a_\parallel)$ and the $\epsilon_\perp = \xi(a_\perp - a_\parallel)/(a_\perp + \xi a_\parallel)$ of the film. For the elastic constants, we adopt the values C_{11} = 128.5 GPa and C_{12} = 48.3 GPa,[32] whereas for strained Ge film, we use $a_{\parallel,Ge}$ = 5.6802 Å and $a_{\perp,Ge}$ = 5.6416 Å obtained from XRD. These data yield parallel and perpendicular strain values of $\epsilon_\parallel \approx +0.40\%$ and $\epsilon_\perp \approx -0.30\%$ and an unstrained Ge lattice constant of a_0 = 5.658 Å, in excellent agreement with the known bulk Ge value. Taking differentials of the strain relations above yields the following expression

$$\frac{\delta\varepsilon_\parallel}{\varepsilon_\parallel} = \left(\frac{1}{1 + a/\xi a_\parallel}\right)\frac{\delta\xi}{\xi} \approx \frac{1}{2}\frac{\delta\xi}{\xi} \qquad (2)$$

Thus a fractional error in the elastic ratio $\xi = 2C_{12}/C_{11}$ produces half this error in the in-plane strain. For instance, if C_{11} = 129 ± 3 GPa and C_{12} = 48 ± 3 GPa,[32] then ξ = 0.75 ± 0.07 (±9.3%), which implies a corresponding fractional error of only ~5% in the in-plane strain. So, for the Ge/$Ge_{0.965}Sn_{0.035}$, we obtain $\varepsilon_\parallel \approx 0.40 \pm 0.03\%$. The corresponding strain value obtained by Raman (see below) is $\varepsilon_\parallel \approx 0.43$, well within the 0.03% error. This value represents the highest tensile strain observed in elemental Ge semiconductors to date.

Extensive XRD studies of a wide range of tensile-strained Ge films grown on $Ge_{1-y}Sn_y$ (y = 0.015–0.035) indicated strain states between 0.15 and 0.43%. The XTEM data of these samples revealed monocrystalline films possessing commensurate interfaces and atomically smooth surfaces regardless of the epilayer thickness. Images a and b in Figure 18 show electron micrographs of the Ge/$Ge_{0.965}Sn_{0.035}$ sample indicating a 60 nm thick Ge layer grown epitaxially on a 230 nm thick $Ge_{1-y}Sn_y$ buffer. The bright-field image shows essentially no penetrating threading defects over an extended lateral range of 1 μm, and the high-resolution micrograph near the Ge/Si interface reveals a sharp, commensurate transition between the epilayer and the buffer. AFM analysis of the sample shows that the surface is predominantly flat, with an rms roughness of ~1.5 nm over a typical 5 × 5

(31) Tolle, J.; Roucka, R.; Chizmeshya, A. V. G.; Kouvetakis, J.; D'Costa, V. R.; Menendez, J. *Appl. Phys. Lett.* **2006**, *88*, 252112.
(32) Madelung, O. *Semiconductors, Landolt Börstein New Series III*; Springer-Verlag: Berlin, NY, 2001.

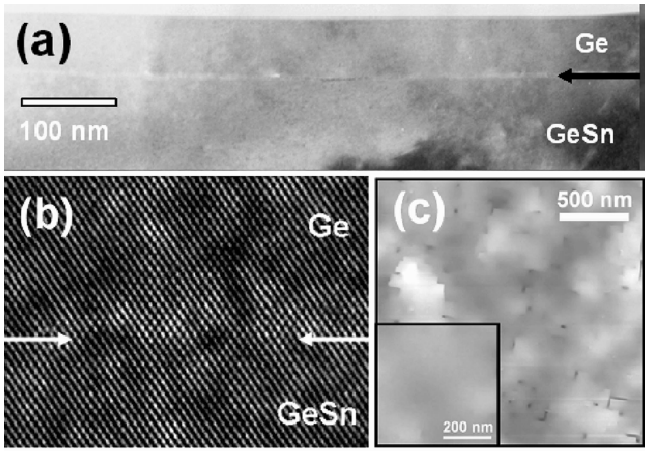

Figure 18. XTEM images of the $Ge/Ge_{0.965}Sn_{0.035}/Si(100)$ heterostructure: (a) diffraction contrast image of Ge/GeSn, (b) high-resolution micrograph of the corresponding interface, (c) $2 \times 2\ \mu m^2$ AFM scan showing a smooth surface created by the coalescence of atomically flat terraces. Inset is a $0.5 \times 0.5\ \mu m^2$ AFM scan with rms roughness of 0.2 nm.

μm^2 area (Figure 18c). On a smaller $0.5 \times 0.5\ \mu m^2$ scale, we observe atomically smooth surfaces with a reduced rms roughness of ~0.2 nm. The difference in these values is associated with the presence of tiny voids located at the intersection of individual coalescing terraces as described previously. In thicker films, these terraces coalesce fully and such features are no longer visible. In contrast, the growth of pure Ge_2H_6 in the absence of the organic additive $(GeH_3)_2CH_2$ produces defective and rough films with classic islandlike surface morphology, consistent with a mismatched heteroepitaxy growth mode. This observation confirms the notion that the organic additives significantly alter the surface energetics, promoting organized assembly of planar Ge films at conditions that would normally preclude their growth directly on GeSn on the basis of surface-energy differences. Note that analogous differences in surface energetics prevent the heteroepitaxial growth of silicon films directly on a Ge surface. However, as we have demonstrated above, the pseudosurfactant properties of the organic additives enable the remarkable and unconventional growth of fully strained and perfectly planar Si layers on Ge buffers.

In addition to XRD, we have used Raman spectroscopy to independently confirm the strains states of the Ge epilayers. In Figure 19a, we show a typical Raman spectrum of the $Ge/Ge_{0.965}Sn_{0.035}$ sample compared to that of a bulk Ge reference. The peak of the Ge film is shifted to lower energies, as expected for tensile strain. The results for this and similar samples are summarized in Figure 19 b, where we plot the Raman shifts of the Ge films with strains intermediate to 0.15 and 0.43% (with respect to the Raman shift in pure Ge) as a function of the measured in-plane strain $\varepsilon_{||}$ obtained from XRD. A monotonic and approximately linear dependence is observed, which confirms the XRD results. A fit with eq 1 yields $b_{Ge} = 436 \pm 18\ cm^{-1}$. This overlaps considerably with the earlier results of Cerdeira et al.[21] Thus we conclude that, as in the case of Si, the original strain shift coefficients determined in the 1970s are sufficiently accurate to characterize strain using Raman spectroscopy. Finally, we note that preliminary photoreflectance studies of selected samples have shown a downshift in the direct gap consistent with tensile strain, offering the prospect of producing direct transitions in elemental Ge at sufficiently high strains approaching 2%.

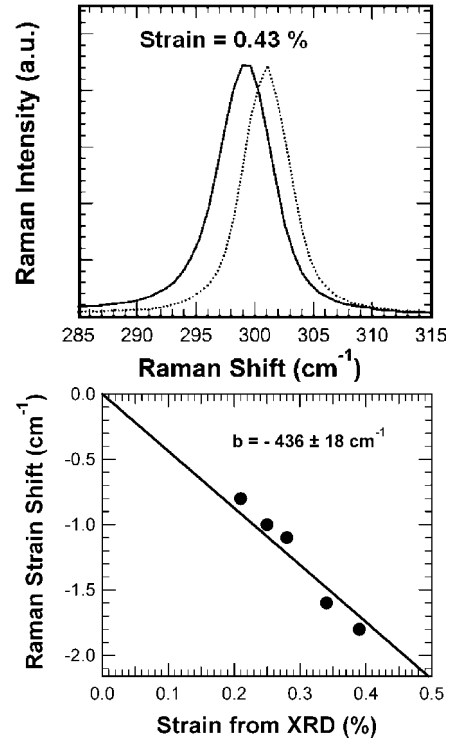

Figure 19. (a) Raman spectrum of $Ge/Ge_{0.965}Sn_{0.035}$ (solid line) and that of a bulk Ge (dotted line) to highlight the strain-induced downshift. (b) In-plane strain-induced Raman shifts in tensile-strained Ge/GeSn films (solid line) as a function of the measured in-plane strain.

Conclusions

We find that $(GeH_3)_2CH_2$ and GeH_3CH_3 with built-in pseudo surfactant capabilities enable growth of atomically flat (rms 0.21 nm) and stress-free Ge films directly on Si. High growth rates are achieved at low temperature (350–420 °C) using Ge_2H_6, and produce perfectly pure films with threading dislocation densities below $1 \times 10^5\ cm^{-2}$ (orders of magnitude less than that attainable from the best competing process available). The desirable growth conditions and low threading dislocation densities make this material suitable for applications in selective growth. Raman studies of these samples confirm that they are virtually stress- and defect-free. The photoreflectance signal is comparable to that of bulk Ge, and in the most perfectly relaxed films, we have also observed photoluminescence.

As a proof of concept application, we have employed this approach to grow selective Ge source/drain structures in prototype devices. Within the context of group IV microelectronic architectures, this strategy provides a practical path to compressively strain Si channels with increased hole mobilities. These Ge buffers should also provide an ideal platform for producing perfectly crystalline and fully epitaxial Si epilayers suitable for high-speed transistor applications. The growth of Si directly on Ge conducted via trisilane also creates opportunities for the development of new Ge-based Metal-Oxide-Semiconductor devices in which thin Si films can act as passivation layers for the growth of high-*k* dielectrics on Ge.

Tensile-strained Ge layers have been deposited at 360–380 °C on Si(100) via fully relaxed $Ge_{1-y}Sn_y$ buffers. XRD and Raman analyses are used extensively to determine the strain properties of these materials. The results indicate that the precise strain state of the epilayers is controlled by varying the Sn content of the buffer ($y = 0.015$–0.035), yielding tunable tensile strains as high as 0.43%. Our approach is straightforward and suitable for large-scale integration. In contrast to strain-tuning via thermal expansion, our process proceeds in a controlled and systematic fashion at low temperatures (∼360 °C) compatible with selective growth and yields record-high tensile strains.

Acknowledgment. This work was supported by the AFOSR MURI, FA9550-06-01-0442. We thank ASM America for supplying the patterned wafers used for selective growth and Shawn Thomas for advice on this topic. We also thank Voltaix Corporation for donating the germane used in this work.

CM071581V